On the physical origin of dark matter density profiles

Y. Ascasibar,[1,2,3] G. Yepes,[2] S. Gottlöber[3] and V. Müller[3]

[1] *Theoretical Physics, 1Keble Road, Oxford OX1 3NP*
[2] *Grupo de Astrofísica, Universidad Autónoma de Madrid, Madrid E-28049, Spain*
[3] *Astrophysikalisches Institut Potsdam, An der Sternwarte 16, Potsdam D-14482, Germany*

2 February 2008

ABSTRACT
The radial mass distribution of dark matter haloes is investigated within the framework of the spherical infall model. We present a new formulation of spherical collapse including non-radial motions, and compare the analytical profiles with a set of high-resolution N-body simulations ranging from galactic to cluster scales. We argue that the dark matter density profile is entirely determined by the initial conditions, which are described by only two parameters: the height of the primordial peak and the smoothing scale. These are physically meaningful quantities in our model, related to the mass and formation time of the halo. Angular momentum is dominated by velocity dispersion, and it is responsible for the shape of the density profile near the centre. The phase-space density of our simulated haloes is well described by a power-law profile, $\rho/\sigma^3 = 10^{1.46\pm0.04}(\rho_c/v_{\rm vir}^3)(r/r_{\rm vir})^{-1.90\pm0.05}$. Setting the eccentricity of particle orbits according to the numerical results, our model is able to reproduce the mass distribution of individual haloes.

Key words: galaxies: haloes – cosmology: theory – dark matter

1 INTRODUCTION

The hierarchical clustering paradigm states that the growth of cold dark matter (CDM) haloes proceeds by accretion of smaller units from the surrounding environment, either by continuous infall or by discrete merging events.

Cosmological N-body simulations are a valuable tool to study the mass distribution of dark matter haloes and its evolution in the non-linear regime. In the early numerical work of Quinn et al. (1986) and Frenk et al. (1988), haloes showed an isothermal density profile ($\rho \propto r^{-2}$). Dubinski & Carlberg (1991) and Crone et al. (1994) had enough resolution in their simulations to detect the first evidence of departure from a pure power-law. Later on, Navarro et al. (1996, 1997, hereafter NFW) found that the density profile could be fitted by a simple analytical function

$$\rho(r) = \frac{\rho_{\rm s}}{(r/r_{\rm s})(1 + r/r_{\rm s})^2} \tag{1}$$

in terms of a characteristic density $\rho_{\rm s}$ and a characteristic radius $r_{\rm s}$. This profile is steeper than isothermal at large radii and shallower near the centre. The logarithmic slope of the density profile, $\alpha(r) \equiv {\rm d}\log(\rho)/{\rm d}\log(r)$, tends to $\alpha = -3$ for $r \to \infty$ and $\alpha = -1$ for $r \to 0$. It corresponds to the isothermal case, $\alpha = -2$, at the characteristic radius only. Navarro et al. (1997) further showed that the two free parameters in equation (1) are not independent. Should this be true, the final mass distribution of objects of different

scales could be described in terms of a one-parameter family of analytical profiles.

Similar results have been found in independent simulations with much higher mass and force resolution than the original NFW paper. However, there is still some controversy about the innermost value of α and its dependence on resolution. Moore et al. (1998, 1999), Ghigna et al. (1998, 2000) and Fukushige & Makino (1997, 2001) find steeper density profiles near the centre ($\alpha \sim -1.5$), whereas other authors (Jing & Suto 2000; Klypin et al. 2001) claim that the actual value of α may depend on halo mass, merger history, and substructure. Power et al. (2003) pointed out that the logarithmic slope becomes increasingly shallow inwards, with little sign of approaching an asymptotic value at the resolved radii. In that case, the precise value of α at a given cut-off scale would not be particularly meaningful. This result has been later confirmed by Fukushige et al. (2003) and Hayashi et al. (2003), and it is predicted by several analytical models (e.g. Taylor & Navarro 2001; Hoeft et al. 2003).

Observed rotation curves of dwarf spiral and LSB galaxies (e.g. Flores & Primack 1994; Moore 1994; Burkert 1995; Kravtsov et al. 1998; Borriello & Salucci 2001; de Blok et al. 2001; de Blok & Bosma 2002; Marchesini et al. 2002) seem to indicate that the shape of the density profile at small scales is significantly shallower than what is found in numerical simulations. This discrepancy has been often signalled as a genuine crisis of the CDM scenario, and several alternatives

have been suggested, such as warm (Colín et al. 2000; Sommer-Larsen & Dolgov 2001), repulsive (Goodman 2000), fluid (Peebles 2000), fuzzy (Hu et al. 2000), decaying (Cen 2001), annihilating (Kaplinghat et al. 2000), or self-interacting (Spergel & Steinhardt 2000; Yoshida et al. 2000; Davé et al. 2001) dark matter.

Unfortunately, it has proved remarkably hard to establish the inner slope of the dark matter distribution observationally (see e.g. Swaters et al. 2003). Some authors (van den Bosch & Swaters 2001; Jimenez et al. 2003; Swaters et al. 2003) claim that a cuspy density profile with $\alpha \leqslant -1$ is consistent with current observations, although a shallower slope is able to explain them as well. Yet, a value as steep as $\alpha = -1.5$ can be confidently ruled out in most cases. According to Hayashi et al. (2003), only about 30 per cent of the rotational curves are actually inconsistent with the simulation data.

On cluster scales, X-ray analyses have led to wide ranging results, from $\alpha = -0.6$ (Ettori et al. 2002) to $\alpha = -1.2$ (Lewis et al. 2003) or even $\alpha = -1.9$ (Arabadjis et al. 2002). Measurements based on gravitational lensing yield conflicting estimates as well, either in rough agreement with the results of numerical simulations (e.g. Dahle et al. 2003; Gavazzi et al. 2003), or finding much shallower slopes, $\alpha = -0.5$ (e.g. Sand et al. 2002, 2003).

A conclusive theoretical prediction of the central mass distribution of CDM haloes is therefore an important check for any model of structure formation. The controversy regarding the 'universal' density profile and its logarithmic slope at the centre has stimulated a great deal of analytical work. On one hand, we would like to find out not only the actual shape of the profile, but also the physical mechanisms behind the 'universality' observed in numerical N-body simulations. On the other hand, it would be interesting to find and explain correlations with halo size, environment, power spectrum or even the nature of dark matter particles.

A number of plausible arguments about the radial structure of CDM haloes have been advanced during the last 30 years. The basic problem of the collisionless collapse of a spherical perturbation in an expanding background was first addressed in the two seminal papers by Gunn & Gott (1972) and Gunn (1977), where the cosmological expansion and the role of adiabatic invariance were first introduced in the context of the formation of individual objects. The next step was accomplished by Fillmore & Goldreich (1984) and Bertschinger (1985), who found analytical predictions for the density of collapsed objects seeded by scale-free primordial perturbations in a flat universe. Hoffman & Shaham (1985) generalised these solutions to realistic initial conditions in flat as well as open Friedmann models. Modifications of the self-similar collapse model to include more realistic dynamics of the growth process have been proposed (e.g. Avila-Reese et al. 1998; Henriksen & Widrow 1999; Łokas 2000; Kull 1999; Subramanian et al. 2000). Several authors (e.g. Syer & White 1998; Salvador-Sole et al. 1998; Nusser & Sheth 1999; Manrique et al. 2003) argue that the central density profile is linked to the merging history of dark matter substructure, and baryons have been invoked both to shallow (e.g. El-Zant et al. 2001, 2003) and to steepen (Blumenthal et al. 1986) the dark matter profile.

In this paper, we present an analytical model for the assembly of CDM haloes based on the spherical col-

lapse paradigm. Following the spirit of Hoffman & Shaham (1985), we will assume that objects do not form around *local* maxima of the primordial density field, but of the *smoothed* density field. We argue that all information about the initial conditions below the smoothing scale is lost during the merging process. We will show that setting the smoothing scale for a halo of a given mass is equivalent to specifying its formation time. Initial conditions are computed following the Gaussian random peaks statistics described by Bardeen et al. (1986, hereafter BBKS), and angular momentum is included in a phenomenological way. Our theoretical predictions are then compared with the results of high-resolution numerical simulations, showing that this model is able to accurately reproduce the mass distribution of individual objects.

The paper is structured as follows. Details of our implementation of spherical collapse are given in Section 2. Numerical experiments are described in Section 3, where both the mass and velocity distributions are investigated. We discuss our results in Section 4, and Section 5 summarises our main conclusions.

2   SPHERICAL COLLAPSE

The assembly of dark matter haloes is a highly non-linear process, and strong simplifying assumptions must be made in order to tackle the problem analytically. Traditionally, there are two complementary paradigms: the spherical infall model (Gunn & Gott 1972) and the Press-Schecter formalism (Press & Schechter 1974), in which mergers play a dominant role (see e.g. Nusser & Sheth 1999; Manrique et al. 2003).

2.1   The model

The most simple way of addressing the problem of structure formation is to assume spherical symmetry. As shown by Tolman (1934) and Bondi (1947), a spherically symmetric solution of the Einstein equations can be easily interpreted in terms of Newtonian dynamics. The equation of motion for a Lagrangian shell enclosing a mass M can be derived from the conservation of energy

$$\epsilon(r) \equiv \frac{E(r)}{m} \equiv \frac{\dot{r}^2}{2} - G\frac{M(r) + \frac{4\pi}{3}\rho_\Lambda r^3}{r} = \epsilon_i(r) \qquad (2)$$

where $r(t)$ is the Lagrangian coordinate, $M(r) = M_i(r_i)$ is the mass contained within the shell, and $\rho_\Lambda \equiv \frac{\Lambda}{8\pi G}$ is the vacuum energy density associated to a cosmological constant. Throughout this paper, the subscript 'i' will be used to denote initial conditions.

If we assume the universe to be homogeneous, the mass is given by $M_i = \frac{4\pi}{3}\Omega_m^i \rho_c^i r_i^3$, where $\rho_c^i \equiv \frac{3H_i^2}{8\pi G}$. Substituting in (2) and making a coordinate transformation

$$r(t) \equiv r_i \alpha(t) \qquad (3)$$

we obtain the Friedmann equation without radiation:

$$\frac{\dot{\alpha}^2}{H_i^2} - \Omega_m^i \alpha^{-1} - \Omega_\Lambda^i \alpha^2 = 1 - \Omega_m^i - \Omega_\Lambda^i. \qquad (4)$$

In a homogeneous universe, $\alpha(t)$ is independent of r_i and plays the role of a uniform cosmic expansion factor.

Our model assumes that structures grow from spherically symmetric perturbations, defined as

$$\Delta_i(r_i) \equiv \frac{M(r_i)}{\frac{4\pi}{3}\Omega_m^i \rho_c^i r_i^3} - 1 \tag{5}$$

with $0 < \Delta_i \ll 1$. These perturbations are introduced at an early epoch a_i by slightly displacing the spherical shells of matter. Keeping only terms to first order in $\Delta_i(r_i)$, the new positions and velocities are given by

$$r_i' \simeq r_i \left(1 - \frac{1}{3}\Delta_i(r_i)\right) \;\; ; \;\; v_i' \simeq H_i r_i \left(1 - \frac{2}{3}\Delta_i(r_i)\right). \tag{6}$$

The mass enclosed by the perturbed shell is still M_i, and the initial specific energy (using $\Omega_m^i \simeq 1$ and $\Omega_\Lambda^i \simeq 0$) is $\epsilon_i \simeq -\frac{5}{6}\Delta_i(H_i r_i)^2$. Energy conservation (2) leads to the equation of motion

$$-\frac{5}{3}\Delta_i \simeq \frac{\dot{\alpha}^2}{H_i^2} - \Omega_m^i \alpha^{-1} - \Omega_\Lambda^i \alpha^2. \tag{7}$$

According to this equation, the evolution of a single spherical shell would be similar to that of a Friedmann universe. For high enough values of Δ_i, the shell reaches a maximum radius r_m at a *turn-around* time t_m and then re-collapses. In an Einstein-de Sitter universe ($\Omega_m = 1$, $\Omega_\Lambda = 0$), equation (7) can be solved analytically, yielding

$$r_m = \frac{3r_i}{5\Delta_i} \;\; ; \;\; t_m = \frac{\pi}{2H_i(5\Delta_i/3)^{3/2}}. \tag{8}$$

This is also a valid approximation for shells reaching their turn-around radius r_m before the cosmological constant term starts to dominate the expansion. Since the shells need at least another t_m to virialise, expression (8) can be applied in a ΛCDM universe to estimate the maximum expansion radius and time for the innermost part of a virialised halo. For the outer shells, the equation of motion (7) must be integrated numerically in order to find the trajectories up to the maximum radius.

In the absence of shell-crossing, shells would reach the origin at $T = 2t_m$. Since they are assumed to be composed of collisionless CDM particles, they would simply pass through the centre, describing an oscillatory motion with amplitude r_m and period T. However, equation (7) holds as long as the enclosed mass M_i remains constant. As a shell re-collapses, its particles will cross the orbits of inner shells, and energy will not be a constant of motion any more.

After turn-around, our model assumes that the particles belonging to a shell oscillate (or, more generally, *orbit*) within the gravitational potential of the dark matter halo. Since CDM particles are expected to spend most of the time in the outermost regions of their orbits (particularly when angular momentum is taken into account), we approximate the mass distribution of the halo by a simple power law

$$M(r) = M_i \left(\frac{r}{r_m}\right)^{\alpha_M(r_m)} \tag{9}$$

where $\alpha_M(r) \equiv d\log M(r)/d\log r$ is the *local* value of the logarithmic slope of the mass profile, evaluated at the maximum radius of the orbit.

At first sight, this might seem similar to the classical approach based on self-similarity (Bertschinger 1985), but in that case the final mass distribution is indeed assumed to be a power law, whereas in our model this ansatz is only an approximation to compute the local potential. The final

mass profile is obtained self-consistently, adding the contributions from all shells, each of them with an individual value of $\alpha_M(r_m)$.

The probability of finding a particle inside radius r is proportional to the fraction of time it spends within r:

$$P(r, r_m) = \frac{1}{t_m} \int_0^r \frac{dx}{v_r(x)} = \frac{1}{t_m} \int_0^r \frac{dx}{\sqrt{\Phi(r_m) - \Phi(x)}}. \tag{10}$$

We evaluate numerically the value of $\alpha_M(r_m)$ in order to compute the potential. Taking different prescriptions, such as an isothermal profile ($\alpha_M = 1$ for every shell) or a Keplerian potential ($\alpha_M = 0$) does not lead to qualitative variations in the probability $P(r, r_m)$ and the resulting mass distribution.

If phase mixing is considered to be efficient, particles initially on the same shell will be spread out from $r = 0$ to $r = r_m$ a short time after t_m. For the sake of simplicity, we will consider that phase mixing is instantaneous, so immediately after turn-around the shell is transformed into a density distribution whose cumulative mass is proportional to $P(r, r_m)$.

This means that recently accreted particles contribute to the mass within $x_m < r_m$ (i.e. shell-crossing). For shells whose maximum radius was x_m, the enclosed mass changes from $M_i(x_m)$ to

$$M(x_m) = M_i(x_m) + M_{add}(x_m) \tag{11}$$

where $M_{add}(x_m)$ accounts for particles belonging to outer shells. To compute $M_{add}(x_m)$ (see Zaroubi & Hoffman 1993), we must integrate the contribution of every shell whose maximum radius is larger than x_m, up to the current turn-around radius R_{ta}:

$$M_{add}(x_m) = \int_{x_m}^{R_{ta}} \frac{dM_i(r)}{dr} P(x_m, r) \, dr. \tag{12}$$

To compute the evolution of the shell after shell-crossing, we apply adiabatic invariance (Gunn 1977). If the potential evolves on a timescale much longer than the orbital period of the inner particles, their dynamics admits an adiabatic invariant

$$J_r = \frac{1}{2\pi} \oint v_r(r) \, dr \tag{13}$$

also known as the radial action. For a power-law potential, the radial action J_r is proportional to $\sqrt{x_m M(x_m)}$. When we increase the mass by an amount M_{add}, the maximum radius of the inner shell must decrease in order to keep J_r constant. The final radius, x_0, is given by the implicit equation $x_0 = F(x_0) x_m$, where

$$F(x_0) = \frac{M_i}{M_i + M_{add}(x_0)} = \frac{M_i}{M_i + M_{add}[F(x_0)x_m]} \tag{14}$$

and whose solution must be obtained numerically for each shell.

To summarise, the numerical procedure to compute the final radius $r_0(t_0)$ of a Lagrangian shell of matter involves the following steps:

(i) Set M_i (or, equivalently, r_i). Start by the outer shell.
(ii) Integrate the equation of motion (7) up to t_m.
(iii) If $t_m > t_0$, the shell is still expanding: $r_0 = r(t_0)$.
(iv) If $t_m < t_0$, solve (14) to compute $r_0 = F(r_0)r_m$, and add the contribution of this shell to $M_{add}(r)$.

(v) Repeat for the next shell towards the centre.

2.2   Initial conditions

The model described above allows us to compute the mass distribution arising from a primordial fluctuation $\Delta_i(r_i)$, but does not say anything about the shape of this function or its physical origin. Never less, it is important to note that the final density profile is entirely determined by this initial condition. Thus, in the spherical collapse paradigm, the case for a universal density profile can be reformulated in terms of universality in the primordial fluctuations that set $\Delta_i(r_i)$.

Hoffman & Shaham (1985) suggested that, according to the hierarchical scenario of structure formation, haloes should collapse around maxima of the *smoothed* density field. The statistics of peaks in a Gaussian random field has been extensively studied in the classical paper by BBKS. A well-known result is the expression for the radial density profile of a fluctuation centered on a primordial peak of arbitrary height:

$$\frac{\langle \delta_f(r) \rangle}{\sigma_0} = \nu \psi(r) - \frac{\theta(\gamma, \gamma\nu)}{\gamma(1-\gamma^2)} \left[\gamma^2 \psi(r) + \frac{R_*^2}{3} \nabla^2 \psi(r) \right] \quad (15)$$

where $\psi(r) \equiv \xi(r)/\sigma_0$ is the normalised two-point correlation function, $\sigma_0 \equiv \xi(0)^{1/2}$ is the rms density fluctuation, and $\nu\sigma_0$ is the height of the peak. The quantities $\gamma \equiv \sigma_1^2/(\sigma_2\sigma_0)$ and $R_* \equiv \sqrt{3}\sigma_1/\sigma_2$ are related to the moments of the power spectrum,

$$\sigma_j^2 \equiv \frac{1}{2\pi^2} \int_0^\infty P(k) \; k^{2(j+1)} \; dk, \quad (16)$$

and the function $\theta(\gamma, \gamma\nu)$ parametrizes the second derivative of the density fluctuation near the peak. BBKS suggest the approximate fitting formula

$$\theta(\gamma, \gamma\nu) \simeq \frac{3(1-\gamma^2) + (1.216 - 0.9\gamma^4)\exp[-\frac{\gamma}{2}(\frac{\gamma\nu}{2})^2]}{\left[3(1-\gamma^2) + 0.45 + \frac{\gamma\nu}{2}\right]^{1/2} + \frac{\gamma\nu}{2}} \quad (17)$$

valid to 1 per cent accuracy in the range $0.4 < \gamma < 0.7$ and $1 < \gamma\nu < 3$, which is the scale relevant for both galaxies and galaxy clusters.

Expression (15) is often quoted in the literature (e.g. Hoffman 1988; Łokas & Hoffman 2000; Del Popolo et al. 2000; Hiotelis 2002) as the initial condition $\Delta_i(r_i)$. However, we argue that $\langle \delta_f(r) \rangle$ denotes the *smoothed* density profile around a local maximum of the smoothed density field,

$$\delta_f(\vec{r}) = \int W_f(\vec{r} - \vec{x}) \delta(\vec{x}) d^3\vec{x} \quad (18)$$

where the function $W_f(\vec{r} - \vec{x})$ is a smoothing kernel that depends on a certain filtering scale R_f.

The smoothed profile $\langle \delta_f(r) \rangle$ given by (15) is in general not equal to the mean value of the actual overdensity, $\delta(r)$, that must be integrated to compute $\Delta_i(r_i)$:

$$\Delta_i(r_i) = 4\pi \int_0^{r_i} \delta(\vec{x}) x^2 dx. \quad (19)$$

Comparing this expression with (18), we see that $\Delta_i(r_i)$ is equivalent to $\delta_f(0)$ as long as W_f is taken to be a spherical top hat of radius r_i.

To sum up, we are interested in the *physical* density profile $\Delta_i(r_i)$ around a local maximum of the *smoothed* density field. To locate the maximum, we use a Gaussian smoothing kernel

$$W_f(\vec{r} - \vec{x}) = (2\pi R_f^2)^{-3/2} \exp\left(-\frac{|\vec{r} - \vec{x}|^2}{2R_f^2}\right) \quad (20)$$

in order to avoid the oscillations in Fourier space that arise from a top hat filter. We set the scale of the fluctuation, R_f, and impose the condition that $r = 0$ is a maximum of $\delta_f(\vec{r})$.

Then, we compute $\Delta_i(r_i) = \delta_{r_i}(0)$ by applying a top hat smoothing of radius r_i. BBKS show that the probability distribution of $\delta_{r_i}(0)$ is a Gaussian with mean

$$\langle \delta_{r_i}(0) \rangle = \nu_f \frac{\sigma_{0h}^2}{\sigma_{0f}} - \frac{\gamma_f \theta(\gamma_f, \nu_f)}{1-\gamma_f^2} \frac{\sigma_{0h}^2}{\sigma_{0f}} \left(1 - \frac{\sigma_{1h}^2}{\sigma_{0h}^2} \frac{\sigma_{0f}^2}{\sigma_{1f}^2}\right). \quad (21)$$

The moments

$$\sigma_{jx}^2 \equiv \frac{1}{2\pi^2} \int_0^\infty P_x(k) \; k^{2(j+1)} \; dk \quad (22)$$

are computed from

$$P_f(k) \equiv P(k) \; \exp\left[-(kR_f)^2\right] \quad (23)$$

and

$$P_h(k) \equiv P(k) \; \exp\left[-\frac{(kR_f)^2}{2}\right] \frac{3[\sin(kr_i) - kr_i\cos(kr_i)]}{(kr_i)^3} \quad (24)$$

where $P(k)$ is the ΛCDM power spectrum that we used to generate the initial conditions for our simulations, evaluated at time a_i.

2.3   Angular momentum

Two decades after the seminal paper by Gunn & Gott (1972), White & Zaritsky (1992) pointed out (see also the pioneering work of Gurevich & Zybin 1988) that angular momentum would prevent the orbits of CDM particles from reaching the origin.

For pure radial orbits, the mass in the centre is dominated by M_{add} (i.e. particles from the outer shells) when the profile at turn-around is shallower than isothermal (Fillmore & Goldreich 1984). The final density distribution is $\rho(r) \propto r^{-2}$, independent on the initial logarithmic slope. More recently, Łokas (2000) and Łokas & Hoffman (2000) found a similar result considering non-self-similar primordial fluctuations based on the peak formalism.

Angular momentum arises in linear theory (White 1984) from the misalignment between the asymmetry of the collapsing region (i.e. the inertia tensor) and the tidal forces it experiences during the linear regime. In addition, violent relaxation (Lynden-Bell 1967) transforms the radial infall energy into random velocity dispersion, which has a tangential component.

The total amount of angular momentum acquired by the system is, however, an open question. The usual approach (Avila-Reese et al. 1998; Nusser 2001; Hiotelis 2002) consists in assigning a specific angular momentum at turn-around

$$j \propto \sqrt{GMr_m}. \quad (25)$$

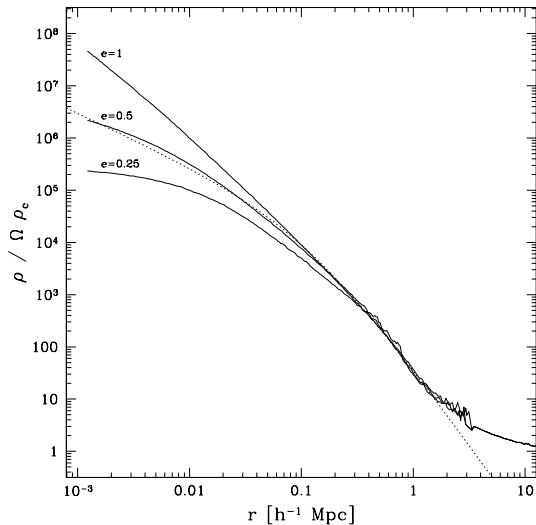With this prescription, the orbit eccentricity e is the

Figure 1. Radial density profile arising from a 3σ fluctuation on $1\ h^{-1}$ Mpc scales (solid lines), for different values of the orbit eccentricity e. A NFW profile (dotted line) is plotted for comparison.

same for all particles in the halo (Nusser 2001). The pericentric radius is given by

$$r_{\min} = \frac{1-e}{1+e}\ r_{\max} \qquad (26)$$

where $r_{\max}$ is computed from adiabatic invariance (14), following the procedure explained in Section 2.1. Angular momentum is taken into account by adding the usual term $j^2/(2r^2)$ to the gravitational potential $\Phi(r)$ in equation (10). Although this changes the actual value of the radial action, J_r is still proportional to $\sqrt{r_{\mathrm{m}} M(r_{\mathrm{m}})}$ and (14) can be used to compute the collapse factor $F(r)$. The assumption of spherical symmetry leads to angular momentum conservation, which implies constant e during the contraction.

The effect of angular momentum is illustrated in Figure 1. We plot the mass distribution at $z = 0$ corresponding to a 3σ peak in the primordial density field, smoothed on $1\ h^{-1}$ Mpc scales. As noted by White & Zaritsky (1992) and Hiotelis (2002), angular momentum plays a key role during secondary infall, decreasing the amount of mass contributed by recently accreted shells in the innermost regions of the halo.

In agreement with Hiotelis (2002), we find that the predicted density profile becomes shallower in the centre as the amount of angular momentum is increased (lower e). Pure radial orbits give rise to a steep profile, somewhat similar to the form proposed by Moore et al. (1999), although the exact shape is slightly different. When the eccentricity is low, the halo develops a constant density core inconsistent with the results of numerical simulations. A value $e = 0.5$ yields a mass distribution virtually indistinguishable from the NFW formula (dotted line in Figure 1) down to kpc scales. However, the logarithmic slope predicted by the model keeps increasing towards the centre, while NFW tends to an asymptotic value, $\alpha = -1$.

3 NUMERICAL EXPERIMENTS

In order to test the analytical model, we carried out a series of high-resolution N-body simulations of cluster formation with the adaptive mesh code ART (Kravtsov et al. 1997). Slightly lower spatial resolution experiments have been run from the same initial conditions with the Tree-SPH gasdynamical code GADGET (Springel et al. 2001; Springel & Hernquist 2002). The radial structure of both dark and baryonic components has been addressed in Ascasibar et al. (2003). For a detailed description of the numerical experiments, the reader is referred to Ascasibar (2003).

A sample of cluster-size haloes has been selected from an initial low-resolution (128^3 particles) pure N-body simulation of a 80 h^{-1} Mpc box in a ΛCDM universe ($\Omega_{\mathrm{m}} = 0.3$; $\Omega_\Lambda = 0.7$; $h = 0.7$; $\sigma_8 = 0.9$). Higher resolution has been achieved by means of the multiple-mass technique (see Klypin et al. 2001, for details), using 3 levels of mass refinement. This is equivalent to an effective resolution of 512^3 CDM particles ($3.1 \times 10^8\ h^{-1}$ M$_\odot$) in the highest refinement level. The minimum cell size allowed in the ART runs was 1.2 h^{-1} kpc. All simulations were started at $z = 50$.

This procedure has been applied to 15 objects, ranging from 3×10^{13} to $2 \times 10^{14}\ h^{-1}$ M$_\odot$. In order to explore a broader mass range, a smaller box (25 h^{-1} Mpc) has been simulated, and six galaxy-size haloes have been added to the cluster sample. Mass resolution is $1.2 \times 10^6\ h^{-1}$ M$_\odot$ for these objects, with a minimum cell size of 0.2 h^{-1} kpc.

All CDM haloes have been classified according to their dynamical state according to a substructure-based criterium. We use the BOUND DENSITY MAXIMA galaxy finding algorithm (see e.g. Colín et al. 1999; Klypin et al. 1999) and look for the most massive subhalo within the virial radius. We label as *major merger* any object in which the subhalo is heavier than 50 per cent the mass of the main object; if the mass is between 10 and 50 per cent, it is classified as a *minor merger*; otherwise, we assume the object to be a *relaxed* system in virial equilibrium.

3.1 Mass distribution

The spherically-averaged mass distribution of our numerical CDM haloes is shown in Figure 2. All profiles have been rescaled by their best-fitting characteristic density and radius. As can be seen in the Figure, the NFW formula provides a reasonable approximation to the mass distribution, although some deviations occur at the innermost part, as well as beyond the virial radius.

In Figure 3, the logarithmic slopes of both mass and density profiles are plotted according to our dynamical classification. We do not find any evidence of an asymptotic behavior up to the resolution limit, in agreement with recent numerical studies (Power et al. 2003; Fukushige et al. 2003; Hayashi et al. 2003). An extrapolation of our results suggests that the central slopes in relaxed haloes could be indeed less steep than the NFW fit, as predicted by analytical models based on the velocity dispersion profile (Taylor & Navarro 2001; Hoeft et al. 2003). More resolution is clearly needed in order to establish a firm conclusion.

As pointed out by several authors (e.g. Jing & Suto 2000; Klypin et al. 2001; Ascasibar et al. 2003), the mass
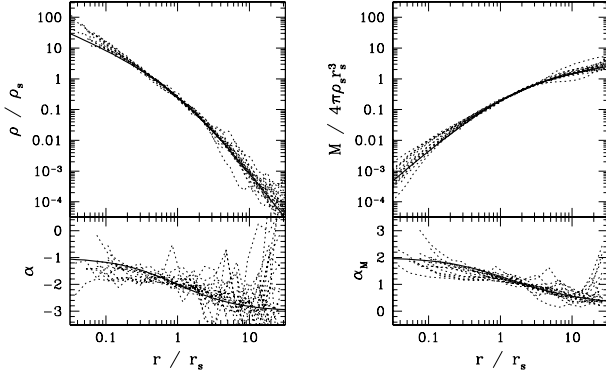
Figure 2. Radial density (left) and mass (right) profiles of our dark matter haloes, rescaled by their best-fitting NFW parameters and plotted as dotted lines. The corresponding logarithmic slopes are shown on the bottom panels. NFW model is indicated by a solid line.
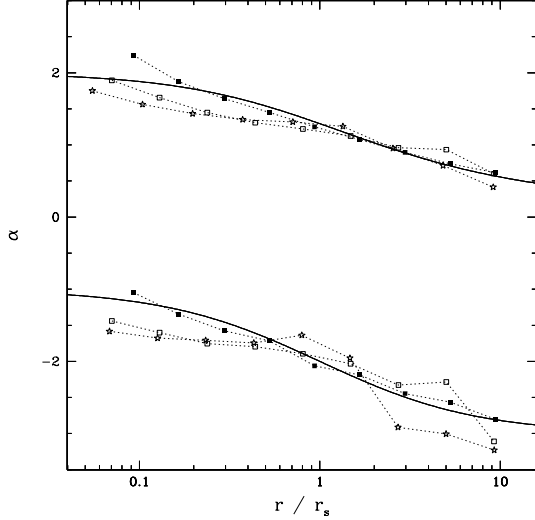

Figure 3. Logarithmic slopes of the mass (top) and density (bottom) profiles. Black squares show the average over relaxed haloes. Minor and major mergers are represented by empty squares and stars, respectively. Solid lines indicate NFW model.

Figure 4. Relation between virial mass and NFW concentration parameter $c \equiv r_{\rm vir}/r_{\rm s}$. Solid squares are used for relaxed systems, empty squares for minor mergers and stars for major mergers. Dashed line shows the model of Bullock et al. (2001). Dotted lines indicate the expected one-sigma scatter.

F of the halo mass at epoch a. According to Bullock et al. (2001), we set $K = 3$ and $F = 0.001$ in order to account for the most massive haloes. The scatter around the relation is fitted by $K = 2$ and $K = 4.7$.

Our sample of dark matter haloes is consistent with the expected trend, although our cluster-size haloes seem to be slightly more concentrated than the theoretical model. On the other hand, major mergers display systematically lower concentrations, since their collapse time is very close to the present. However, the value of a_c is not well defined in a merging system. In particular, during the first stages of the merger the profile corresponds to an old object, perturbed by an approaching satellite. It is only after virialisation when the profile relaxes to its final form, and a_c increases accordingly.

3.2 Angular momentum

In addition to the radial mass distribution, the kinetic structure of numerical haloes can offer interesting insights into the formation of galaxies and galaxy clusters. In particular, we are interested in the specific angular momentum of dark matter particles in order to set the eccentricity in the analytical model.

We separate the velocity field into a random component (i.e. velocity dispersion) and ordered rotation (i.e. average j). The velocity dispersion of a collisionless CDM halo is related to the total mass distribution by virtue of the Jeans equation (see e.g. Binney & Tremaine 1987). For a spherically symmetric system with isotropic velocity dispersion, neglecting infall,

$$\frac{1}{\rho}\frac{{\rm d}(\rho\sigma_r^2)}{{\rm d}r} = -\frac{GM}{r} \qquad (28)$$

where ρ is the local density, σ_r is the radial velocity dispersion, and M is the mass enclosed within radius r. An approximate velocity dispersion profile could be derived by

distribution near the centre might depend on the dynamical state of the halo. At the resolution of the present simulations, relaxed haloes are well described by NFW model, but merging systems display steeper profiles. A conjecture that deserves further investigation is whether violent relaxation and subsequent equipartition of energy may drive the inner part of the system into a nearly isothermal state. That would provide a natural mechanism for the final profile to be independent on the details of the merging history.

Another difference between merging and relaxed systems is that mergers are typically more extended than relaxed haloes of the same mass. We plot in Figure 4 the mass-concentration relation for our sample, compared to the model of Bullock et al. (2001),

$$c(M,a) = K\frac{a}{a_c(M)} \qquad (27)$$

where the collapse time a_c is defined as the epoch at which the typical collapsing mass, $M_*(a_c)$, equals a fixed fraction
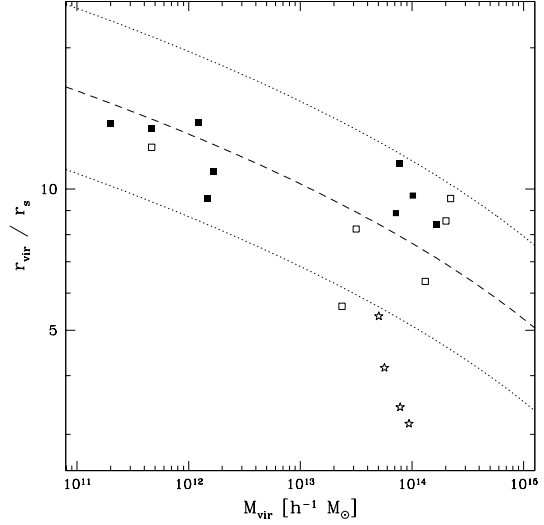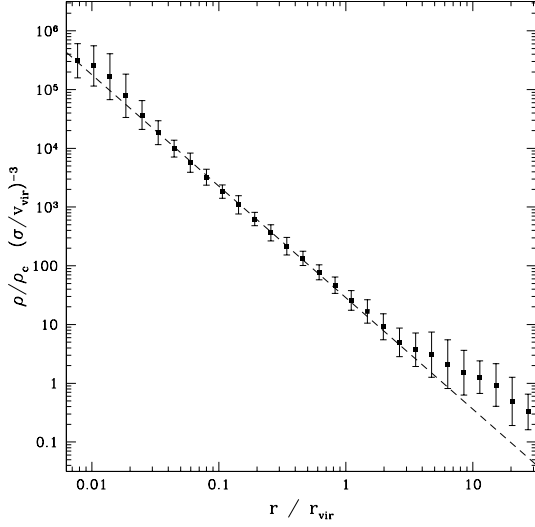
Figure 5. Phase-space density profiles of our haloes (dots). Error bars show the rms scatter of individual profiles around the average. The best-fit 'universal' profile (30) is plotted as a dashed line.

Figure 6. Contribution of bulk rotation (solid squares) and random motions (empty squares) to the tangential velocity of dark matter particles. Points represent the average over all haloes, and error bars indicate the rms scatter.

substituting a given mass distribution (e.g. NFW) and setting an arbitrary normalisation $\sigma_r(0)$. The contribution of random motions to the angular momentum of the CDM particles would be given by the tangential velocity dispersion. In the isotropic case, this amounts to $\left\langle j^2 \right\rangle = 2r^2\sigma_r^2(r)$. Note that random motions do not contribute to the total angular momentum of the halo (i.e. $\langle j \rangle = 0$).

A more empirical approach to the velocity dispersion profile has been followed by Taylor & Navarro (2001). They realised that the coarse-grained phase-space density of a sample of numerical galaxy-size haloes followed a power law

$$\frac{\rho}{\sigma^3} \propto r^\beta \tag{29}$$

with $\beta = -1.875$ over more than two and a half decades in radius. Rasia et al. (2003) obtained a similar result for cluster-size haloes, although their best-fitting slope is $\beta = -1.95$. The normalisation, though, has not been given in any of the two studies.

We have investigated the phase-space structure of the CDM haloes in our sample, including both galaxies and galaxy clusters. The average profile ρ/σ^3 is plotted in Figure 5. We find that all our haloes are well described by

$$\frac{\rho}{\sigma^3} = 10^{1.46\pm0.04} \frac{\rho_c}{v_{\rm vir}^3} \left(\frac{r}{r_{\rm vir}}\right)^{-1.90\pm0.05} \tag{30}$$

where $v_{\rm vir}^2 \equiv GM_{\rm vir}/r_{\rm vir}$. This result is in fair agreement with the slopes reported by Taylor & Navarro (2001) and Rasia et al. (2003). The scatter around the average profile is remarkably low, taking into account that our haloes span four orders of magnitude in mass, and that we considered all systems (even major mergers) in the analysis. Indeed, we do not find any evidence that the slope of the relation depends on mass or dynamical state. Therefore, we claim that expression (30) can be regarded as a 'universal' phase-space density profile with only one free parameter, which is the virial radius of the halo.

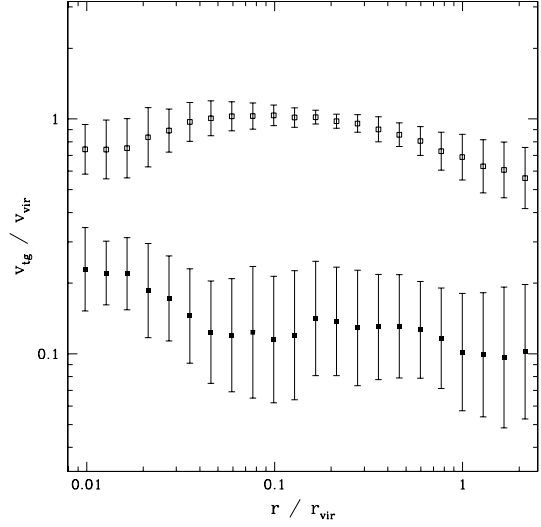We now show in Figure 6 that angular momentum is indeed dominated by random motions. We compare the

contribution to the tangential velocity of CDM particles from $< j >$ and $< j^2 >$ over spherical shells. The average bulk rotation velocity of our halos (solid symbols in Figure 6) is about $0.1v_{\rm vir}$, although we find a significant increase near the centre. Never the less, it is worth mentioning that the separation in bulk and random velocity is prone to numerical errors at the innermost regions. The specific angular momentum grows roughly linearly with radius (rigid body rotation), in agreement with previous numerical work (Barnes & Efstathiou 1987; Bullock et al. 2001; van den Bosch et al. 2002; Chen & Jing 2002). In any case, the tangential velocity of individual dark matter particles is always dominated by the velocity dispersion, for all haloes, at any radius.

As was discussed in Section 2.3, the orbit eccentricity is an important ingredient of our analytical model, since it measures how deep a CDM particle is able to penetrate within the gravitational potential. The ideal case $e = 0$ corresponds to a configuration in which all particles would orbit at constant radius with no mixing between concentric shells, while $e = 1$ (often assumed in spherical infall models) implies that every particle goes through the very centre of mass of the halo. For large values of the eccentricity, the central regions are mainly composed of particles coming from the outer shells, that happen to be near the pericentre of their orbits.

The eccentricity profile of our haloes is plotted in Figure 7. For each object, we compute the spherically-symmetric potential derived from its mass distribution. The pericentric and apocentric radii of every CDM particle are estimated from its position and velocity, and the eccentricity is computed as

$$e = \frac{r_{\rm max} - r_{\rm min}}{r_{\rm max} + r_{\rm min}}. \tag{31}$$

The general trend is that particle orbits are slightly more radial as we move out to the current turn-around radius of the halo, $R_{\rm ta}$. Moreover, we find a systematic dependence on the dynamical state. As can be seen in Figure 8,
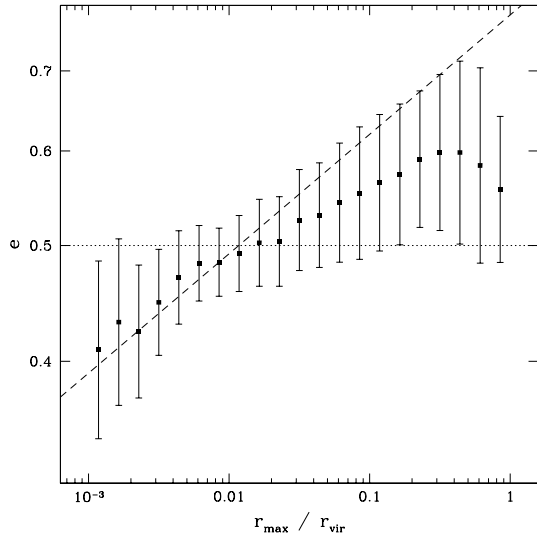
Figure 7. Orbit eccentricity of CDM particles as a function of apocentric radius. Dotted line marks $e = 0.5$; dashed line, expression (32).
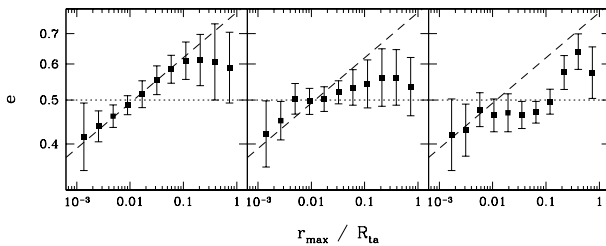

Figure 8. Same as Figure 7, separating relaxed haloes (left), minor (middle) and major (right) mergers.

major mergers are well described by constant eccentricity up to the virial radius [1], while relaxed systems are more consistent with a power-law profile. Minor mergers are somewhat in the middle. The average profile can be fitted by a power law, but the slope is shallower than for relaxed systems.

A least-square fit to the relaxed population yields

$$e(r_{max}) \simeq 0.8 \left(\frac{r_{max}}{R_{ta}} \right)^{0.1} \tag{32}$$

for $r_{max} < 0.1 R_{ta}$. We note that our approximation to compute the eccentricity breaks down at larger radii, since the mass distribution (and thus, the gravitational potential) are by no means static beyond the virial radius.

4   MODEL RESULTS

We now attempt to reproduce the density profiles of our simulated haloes with the model described in Section 2. In order to keep the number of free parameters to a minimum, we assumed a constant eccentricity, $e \simeq 0.5$, which corresponds to the average over the whole radial range. This value implies that particles are able to sink into the dark matter potential

---

[1] For our dark matter haloes, r_{vir}/R_{ta} is typically of the order of $0.2 - 0.3$.
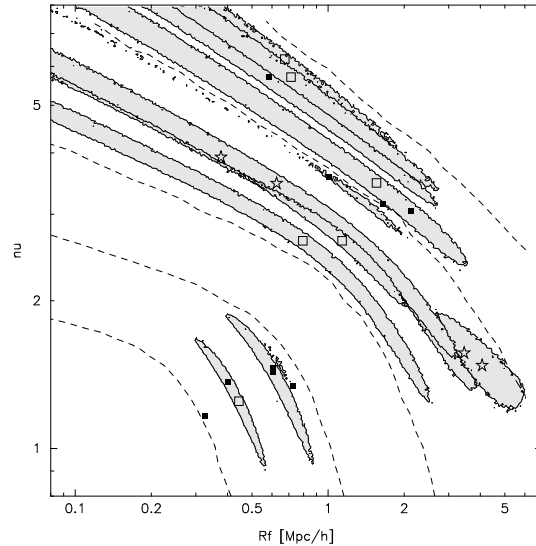

Figure 9. Best-fitting values of the peak height, ν, and the smoothing scale, R_f. Black squares represent relaxed haloes, open squares are used for minor mergers, and stars for major merging systems. Shaded areas indicate $\sqrt{\chi^2/(dof)} \leqslant 0.12$. Dashed lines are drawn at constant r_{vir}.

up to one third of their maximum radius, or, equivalently, that all mass within radius r comes from shells whose turn-around radius was $\leqslant 3r$. The effect of a power law profile will be considered in Section 4.2.

4.1   Constant eccentricity

Once the eccentricity is set to $e = 0.5$, the model has two free parameters, which describe the primordial density peak: its height, ν, and the smoothing scale, R_f. These parameters set the mass and formation time of the halo. For a given mass, a higher peak on a smaller scale corresponds to an earlier formation time and a steeper density profile near the centre.

For each halo, we performed a χ^2 minimisation of the mass profile. Best-fitting values of R_f and ν are plotted in Figure 9, as well as the areas where $\sqrt{\chi^2/(dof)} \leqslant 0.12$. Most cluster-size haloes can be described as very high-ν peaks, while galaxies seem to have collapsed around less extreme fluctuations. This means that clusters are expected to form *earlier* than galaxies, in the sense that the seeds of their dark matter haloes are already in place at a higher redshift.

An exception to this rule are major mergers. While some of these systems still have an early collapse time, some others have collapsed approximately at the present epoch. The first class corresponds to objects that have not relaxed yet, and their core still corresponds to the old halo. As relaxation completes and substructure is erased, the best-fitting parameters move along the lines of constant mass in the $\nu - R_f$ diagram. The smoothing scale rises sharply, and ν decreases accordingly.

As can be seen in Figure 9, there is never the less a certain degeneracy between R_f and ν, which prevents a reliable determination of the formation time. The exact value of the best-fitting parameters may vary within the shaded area, depending on the details of the fit. For instance, we
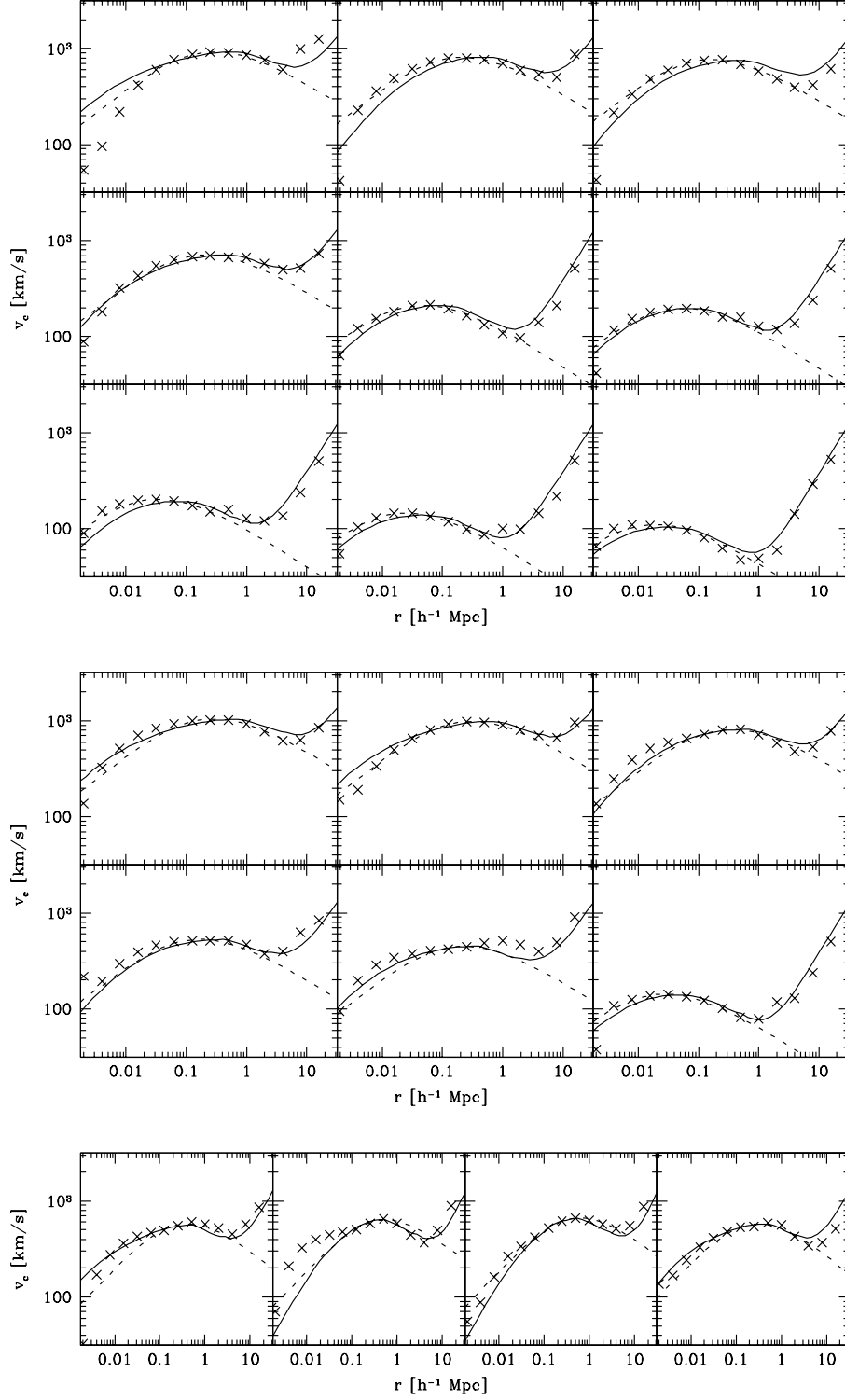
Figure 10. Circular velocity profiles, $v_c^2 \equiv GM/r$. Crosses correspond to the simulation data, while dotted lines are the best-fitting NFW model and solid lines the best-fitting spherical collapse model. Relaxed haloes, minor and major mergers are plotted on the top, middle and bottom panels, respectively.

tend to get higher peaks on smaller scales as we give more weight to the inner parts of the profile.

This can be understood when we compare the numerical data with the results of our spherical collapse model. We chose to fit the radial range $0.1 < r/r_{\rm vir} < 1$ in order to test

the quality of the extrapolations, both towards the centre and to large radii. Individual circular velocity profiles are shown in Figure 10, together with the best fits provided by our model and NFW formula.

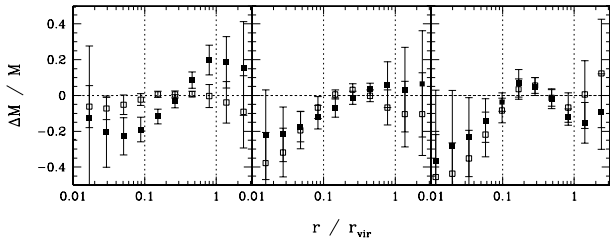Although the mass distribution is fairly well described

Figure 11. Accuracy of NFW (open squares) and spherical collapse (solid) models. Symbols correspond to the average over haloes classified as relaxed (left panel), minor (middle) or major mergers (right). Error bars indicate one-σ scatter of individual profiles, and vertical dotted lines show the radial range used for the fit.

in general terms, the central density is usually underestimated by both models. When we fit the innermost parts, we are biased towards more concentrated distributions. Indeed, if only data within $0.1r_{\rm vir}$ are considered, the best-fitting profiles are rather unrealistic.

At large radii, the spherical collapse model reproduces the upturn in the circular velocity, while NFW drops to zero. This is due to the fact that the density in the NFW model vanishes at infinity, while it tends asymptotically to the mean value in the spherical collapse model. Adding a constant density background to the NFW formula is enough to bring the profile in agreement with the numerical data.

We assess the accuracy of both NFW and spherical collapse models in Figure 11, where the quantity

$$\frac{\Delta M}{M} \equiv \frac{M_{\rm model} - M_{\rm data}}{M_{\rm data}} \qquad (33)$$

is plotted as a function of radius.

The most important difference between both models is that the accuracy of NFW fit improves significantly for relaxed systems, particularly concerning the extrapolation towards $r \to 0$. The fits based on our spherical collapse model are on average less accurate, and the scatter between individual dark matter haloes is a little bit larger. Yet, the uncertainty is always lower than 20 per cent for relaxed objects, and only slightly larger for merging systems, where the prediction of the spherical collapse model is indeed very similar to the NFW fit.

4.2 Variable eccentricity

Although constant eccentricity might provide a useful approximation for merging systems, it is evident from Figure 8 that it is not a good description of relaxed haloes, where the eccentricity profile $e(r)$ increases significantly from the centre to the turn-around radius. Moreover, the assumption of constant eccentricity leads to systematic differences between the mass distribution predicted by our model and the numerical data, as shown in Figure 11.

Therefore, we would like to investigate the consequences of using a more elaborate prescription for $e(r)$. For constant eccentricity, high values of e lead to steeper density profiles in the central regions, whereas the outer parts of the halo remain largely unaffected (see Figure 1). We plot in Figure 12 the density profile resulting from our power-law fit (32) for $\nu = 3$ and $R_{\rm f} = 1 \ h^{-1}$ Mpc. The mass distribution
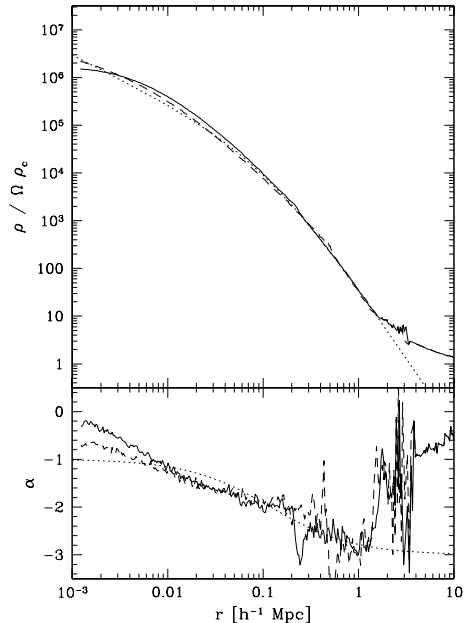

Figure 12. Comparison between a NFW density profile (dotted line), the spherical collapse model with constant eccentricity $e = 0.5$ (dashed line), and a power-law $e(r)$ given by (32) (solid line). Top panel displays the density profile, and bottom panel its logarithmic slope.
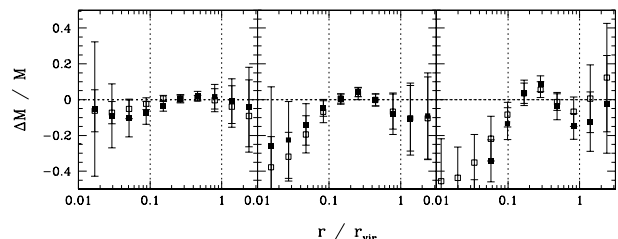

Figure 13. Same as Figure 11, when the eccentricity is set according to (32).

is very similar to that obtained with $e = 0.5$, but the shape is slightly different. There is a small increase in the density between 10 and 100 h^{-1} kpc, but the profile flattens near the centre due to the more circular orbits.

This flattening can be clearly seen on the bottom panel of Figure 12, where we plot the logarithmic slope of the density profile. It is interesting to note that the spherical collapse model predicts a finite density at $r = 0$ when non-radial motions are included, albeit the size of the 'core' is extremely small. As was discussed in Section 3.1, a similar trend is shown by the relaxed haloes in our sample.

At our resolution limit, the net effect of using expression (32) is just to increase the density at small radii. Then our model gives a somewhat poorer description of merging systems, but the quality of the fit improves considerably for relaxed haloes. As can be seen in Figure 13, the accuracy of our model is comparable to NFW formula when a realistic prescription is used for the eccentricity of particle orbits.

5 DISCUSSION AND CONCLUSIONS

The radial density profile of dark matter haloes has been investigated within the framework of the spherical collapse theory. We have shown that the model described in Section 2 is able to reproduce the mass distribution of realistic CDM haloes. Although the final profile cannot be cast in a simple analytical form, it provides not only a mere phenomenological fit, but a physically-motivated description of the density distribution in terms of the primordial initial conditions.

However, it is not easy to understand how the assumption of spherical symmetry could be able to describe the hierarchical assembly of cosmological structures. Instead of continuous infall of spherical shells, the formation of CDM haloes observed in numerical experiments takes place in a discrete and anisotropic way. Most of the matter is accreted in clumps, along the preferred directions set by the filamentary large scale structure.

None the less, the very complicated coalescence process looks very regular in energy space (Zaroubi et al. 1996). Moreover, Moore et al. (1999) have shown that the final density profile is not very sensitive to the details of the merging history, by comparing the mass distribution of a galaxy cluster halo with a re-simulation in which the power spectrum was truncated at ~ 4 Mpc scales.

We suggest, as a plausible explanation for the success of the spherical infall model, that merging is implicitly taken into account through the smoothing scale R_f. Cosmological structures do not form around maxima of primordial density field, but of the *smoothed* density field (Hoffman & Shaham 1985). Some memory of the initial conditions will be lost during major mergers, particularly at the innermost regions of the resulting halo. Contrary to the common view (see e.g. BBKS), we argue that R_f has a precise physical interpretation; below the mass scale defined by R_f, all information about the primordial substructure would have been erased by relaxation processes.

In the outer regions, matter is accreted in a more gentle way. Minor mergers do not significantly alter the dynamical structure of the halo. The mass of infalling clumps is much less than the average over a spherical shell at large radii. Thus, the density profile and the accretion rate are determined by the amount of matter available to the halo, which is ultimately set by the primordial initial conditions.

Never the less, there is still an additional degree of freedom, related to the amount and distribution of angular momentum within the dark matter halo. Angular momentum sets the shape of the density profile at the inner regions. For pure radial orbits, the core is dominated by particles from the outer shells. As the angular momentum increases, these particles remain closer to their maximum radius, resulting in a shallower density profile.

We found that angular momentum is dominated by the tangential component of the velocity dispersion. Random motions are well described by a 'universal' phase-space density profile over several orders of magnitude in radius. This profile is a power law with slope $\beta \simeq -1.9$, in agreement with the results of Taylor & Navarro (2001) for galactic-size haloes and Rasia et al. (2003) for clusters. We found that this profile is valid for all objects in our sample (spanning a mass range from 10^{11} to 10^{15} $M_\odot$) as long as the virial radius is used as a scale parameter.

Although it would be desirable to establish a link between the initial conditions and the specific angular momentum, we resorted to a phenomenological approach. According to the results of our numerical simulations, the orbit eccentricity can be set to a constant value of $e = 0.5$ as a first order approximation. However, relaxed haloes are better described by a power-law profile in terms of their turn-around radius. The details of the mass distribution depend only moderately on the prescription assumed for the angular momentum. Therefore, the spherical collapse model provides a valuable tool to predict the structure of virialised dark matter haloes, given the power spectrum of primordial fluctuations. Indeed, we claim that the physical origin of the mass distribution observed at the present day is related to the shape of the primordial density peaks. 'Universal' profiles with two free parameters arise naturally from Gaussian random peak statistics, since the primordial fluctuations are fully specified by their height, ν, and smoothing scale, R_f.

REFERENCES

Arabadjis J. S., Bautz M. W., Garmire G. P., 2002, ApJ, 572, 66

Ascasibar Y., 2003, PhD thesis, Universidad Autónoma de Madrid (Spain), (astro-ph/0305250)

Ascasibar Y., Yepes G., Müller V., Gottlöber S., 2003, MN-RAS, submitted (astro-ph/0306264)

Avila-Reese V., Firmani C., Hernández X., 1998, ApJ, 505, 37

Bardeen J. M., Bond J. R., Kaiser N., Szalay A. S., 1986, ApJ, 304, 15

Barnes J., Efstathiou G., 1987, ApJ, 319, 575

Bertschinger E., 1985, ApJS, 58, 39

Binney J., Tremaine S., 1987, Galactic dynamics. Princeton, NJ, Princeton University Press, 1987, 747 p.

Blumenthal G. R., Faber S. M., Flores R., Primack J. R., 1986, ApJ, 301, 27

Bondi H., 1947, MNRAS, 107, 410

Borriello A., Salucci P., 2001, MNRAS, 323, 285

Bullock J. S., Dekel A., Kolatt T. S., Kravtsov A. V., Klypin A. A., Porciani C., Primack J. R., 2001, ApJ, 555, 240

Burkert A., 1995, ApJ, 447, L25

Cen R., 2001, ApJ, 546, L77

Chen D. N., Jing Y. P., 2002, MNRAS, 336, 55

Colín P., Avila-Reese V., Valenzuela O., 2000, ApJ, 542, 622

Colín P., Klypin A. A., Kravtsov A. V., Khokhlov A. M., 1999, ApJ, 523, 32

Crone M. M., Evrard A. E., Richstone D. O., 1994, ApJ, 434, 402

Dahle H., Hannestad S., Sommer-Larsen J., 2003, ApJ, 588, L73

Davé R., Spergel D. N., Steinhardt P. J., Wandelt B. D., 2001, ApJ, 547, 574

de Blok W. J. G., Bosma A., 2002, A&A, 385, 816

de Blok W. J. G., McGaugh S. S., Bosma A., Rubin V. C., 2001, ApJ, 552, L23

Del Popolo A., Gambera M., Recami E., Spedicato E., 2000, A&A, 353, 427

Dubinski J., Carlberg R. G., 1991, ApJ, 378, 496

El-Zant A., Hoffman Y., Primack J., Combes F., Shlosman I., 2003, ApJ, submitted (`astro-ph/0309412`)

El-Zant A., Shlosman I., Hoffman Y., 2001, ApJ, 560, 636

Ettori S., Fabian A. C., Allen S. W., Johnstone R. M., 2002, MNRAS, 331, 635

Fillmore J. A., Goldreich P., 1984, ApJ, 281, 1

Flores R. A., Primack J. R., 1994, ApJ, 427, L1

Frenk C. S., White S. D. M., Davis M., Efstathiou G., 1988, ApJ, 327, 507

Fukushige T., Kawai A., Makino J., 2003, ApJ, submitted (`astro-ph/0306203`)

Fukushige T., Makino J., 1997, ApJ, 477, L9

Fukushige T., Makino J., 2001, ApJ, 557, 533

Gavazzi R., Fort B., Mellier Y., Pelló R., Dantel-Fort M., 2003, A&A, 403, 11

Ghigna S., Moore B., Governato F., Lake G., Quinn T., Stadel J., 1998, MNRAS, 300, 146

Ghigna S., Moore B., Governato F., Lake G., Quinn T., Stadel J., 2000, ApJ, 544, 616

Goodman J., 2000, New Astronomy, 5, 103

Gunn J. E., 1977, ApJ, 218, 592

Gunn J. E., Gott J. R. I., 1972, ApJ, 176, 1

Gurevich A. V., Zybin K. P., 1988, Zhurnal Eksperimental noi i Teoreticheskoi Fiziki, 94, 3

Hayashi E., Navarro J. F., Power C., Jenkins A., Frenk C. S., White S. D. M., Springel V., Stadel J., Quinn T., 2003, MNRAS, submitted (`astro-ph/0310576`)

Henriksen R. N., Widrow L. M., 1999, MNRAS, 302, 321

Hiotelis N., 2002, A&A, 382, 84

Hoeft M., Mücket J. P., Gottlöber S., 2003, ApJ, in press

Hoffman Y., 1988, ApJ, 329, 8

Hoffman Y., Shaham J., 1985, ApJ, 297, 16

Hu W., Barkana R., Gruzinov A., 2000, Physical Review Letters, 85, 1158

Jimenez R., Verde L., Oh S. P., 2003, MNRAS, 339, 243

Jing Y. P., Suto Y., 2000, ApJ, 529, L69

Kaplinghat M., Knox L., Turner M. S., 2000, Physical Review Letters, 85, 3335

Klypin A., Gottlöber S., Kravtsov A. V., Khokhlov A. M., 1999, ApJ, 516, 530

Klypin A., Kravtsov A. V., Bullock J. S., Primack J. R., 2001, ApJ, 554, 903

Kravtsov A. V., Klypin A. A., Bullock J. S., Primack J. R., 1998, ApJ, 502, 48

Kravtsov A. V., Klypin A. A., Khokhlov A. M., 1997, ApJS, 111, 73

Kull A., 1999, ApJ, 516, L5

Lewis A. D., Buote D. A., Stocke J. T., 2003, ApJ, 586, 135

Łokas E. L., 2000, MNRAS, 311, 423

Łokas E. L., Hoffman Y., 2000, ApJ, 542, L139

Lynden-Bell D., 1967, MNRAS, 136, 101

Manrique A., Raig A., Salvador-Solé E., Sanchis T., Solanes J. M., 2003, ApJ, 593, 26

Marchesini D., D'Onghia E., Chincarini G., Firmani C., Conconi P., Molinari E., Zacchei A., 2002, ApJ, 575, 801

Moore B., 1994, Nature, 370, 629

Moore B., Governato F., Quinn T., Stadel J., Lake G., 1998, ApJ, 499, L5

Moore B., Quinn T., Governato F., Stadel J., Lake G., 1999, MNRAS, 310, 1147

Navarro J. F., Frenk C. S., White S. D. M., 1996, ApJ, 462, 563

Navarro J. F., Frenk C. S., White S. D. M., 1997, ApJ, 490, 493

Nusser A., 2001, MNRAS, 325, 1397

Nusser A., Sheth R. K., 1999, MNRAS, 303, 685

Peebles P. J. E., 2000, ApJ, 534, L127

Power C., Navarro J. F., Jenkins A., Frenk C. S., White S. D. M., Springel V., Stadel J., Quinn T., 2003, MNRAS, 338, 14

Press W. H., Schechter P., 1974, ApJ, 187, 425

Quinn P. J., Salmon J. K., Zurek W. H., 1986, Nature, 322, 329

Rasia E., Tormen G., Moscardini L., 2003, ApJ, submitted (`astro-ph/0309405`)

Salvador-Sole E., Solanes J. M., Manrique A., 1998, ApJ, 499, 542

Sand D. J., Treu T., Ellis R. S., 2002, ApJ, 574, L129

Sand D. J., Treu T., Smith G. P., Ellis R. S., 2003, ApJ, submitted (`astro-ph/0309465`)

Sommer-Larsen J., Dolgov A., 2001, ApJ, 551, 608

Spergel D. N., Steinhardt P. J., 2000, Physical Review Letters, 84, 3760

Springel V., Hernquist L., 2002, MNRAS, 333, 649

Springel V., Yoshida N., White S. D. M., 2001, New Astronomy, 6, 79

Subramanian K., Cen R., Ostriker J. P., 2000, ApJ, 538, 528

Swaters R. A., Madore B. F., van den Bosch F. C., Balcells M., 2003, ApJ, 583, 732

Syer D., White S. D. M., 1998, MNRAS, 293, 337

Taylor J. E., Navarro J. F., 2001, ApJ, 563, 483

Tolman R. C., 1934, Proceedings of the National Academy of Science, 20, 169

van den Bosch F. C., Abel T., Croft R. A. C., Hernquist L., White S. D. M., 2002, ApJ, 576, 21

van den Bosch F. C., Swaters R. A., 2001, MNRAS, 325, 1017

White S. D. M., 1984, ApJ, 286, 38

White S. D. M., Zaritsky D., 1992, ApJ, 394, 1

Yoshida N., Springel V., White S. D. M., Tormen G., 2000, ApJ, 544, L87

Zaroubi S., Hoffman Y., 1993, ApJ, 416, 410

Zaroubi S., Naim A., Hoffman Y., 1996, ApJ, 457, 50